

# Life Products of Stars

Aldo M. Serenelli

*Institute for Advanced Study, Einstein Drive, Princeton, NJ 08540, USA*

and

Masataka Fukugita

*Institute for Advanced Study, Einstein Drive, Princeton, NJ 08540, USA*

*Institute for Cosmic Ray Research, University of Tokyo, Kashiwa 277-8582, Japan*

## ABSTRACT

We attempt to document complete energetic transactions of stars in their life. We calculate photon and neutrino energies that are produced from stars in their each phase of evolution from 1 to  $8M_{\odot}$ , using the state-of-the-art stellar evolution code, tracing the evolution continuously from pre-main sequence gravitational contraction to white dwarfs. We also catalogue gravitational and thermal energies and helium, and heavier elements that are stored in stars and those ejected into interstellar space in each evolutionary phase.

*Subject headings:* stars: fundamental parameters – stars: mass loss – stars: evolution

## 1. Introduction

Stars are taken as an engine that uses hydrogen as a fuel, producing energy mostly in photons and leaving helium and heavier elements as ashes. Baryons in stars are only 6% of those in the Universe, yet stars cause varieties of most spectacular phenomena, and also give a key to understanding the energetics of the Universe (Fukugita & Peebles 2004; hereafter FP). FP presented an accounting of energies that are relevant to stars using rather rough estimates in view of the difficulty in assembling the relevant astrophysical quantities. There are many calculations of stellar evolution done to date, some of the most recent examples being the Geneva tracks (Schaller et al. 1992; Charbonnel et al. 1996) and the Padova tracks (Girardi et al. 2000) among others, but quantities like integrated luminosities and gravitational binding energies stored in stars are not explicitly presented.

The purpose of this paper is to present evolution of stars mainly from the energetics point of view. For example, how much radiation energy is produced in main sequence phase, how much in red giant branch and asymptotic branch phases, and

how much energy is stored in heavy elements as well as in gravitational binding, and so forth? The energies in radiation observed in the extragalactic background light must balance those produced by stars besides a small fraction contributed by active galactic nuclei, and they are documented in the nuclear binding energy as a fossil record. We also want to know how much fraction of helium and heavy element produced in stars are liberated into interstellar space. Then, what fraction of energies go to neutrinos, which account for the difference between the nuclear binding energy and the energy in radiation?

We focus our calculations on low and intermediate mass stars from 1 to 8 solar masses that eventually end up as white dwarfs, and we follow the evolution from pre-main sequence contraction to the cool white dwarf with luminosity  $\log(L/L_{\odot}) = -4.5$ . This enables us to compute integrated output of stars in a consistent way. We also add the case for  $0.8M_{\odot}$ , calculated to the beginning of helium ignition to allow a continuation to lower mass stars. We consider stars with solar metallicity.

We remark that white dwarfs are the most important reservoir of heavy elements today, which stores about 80% of heavy element in the Universe. The gravitational binding energy stored in white dwarfs is 5 times that in main sequence stars in the cosmic mean. Stellar winds in the thermal-pulse (TP) AGB phase are also the important source of chemical enrichment besides supernovae. Thus, white dwarfs are one of the most prominent fossil records of energy transactions in the Universe (FP).

## 2. Calculations

Calculations have been carried out with the LPCODE stellar evolution code (Althaus et al. 2003). For this work, we have adopted an extended nuclear network involving 32 isotopes from  $^1\text{H}$  to  $^{32}\text{P}$  linked by 96 reactions that cover all relevant nuclear processes from detailed hydrogen and helium burning up to a simplified yet energetically accurate treatment of carbon and neon burning. The NACRE compilation (Angulo et al. 1999) gives the basic set of nuclear reaction rates adopted in this work. The two key reactions  $^{14}\text{N}(p, \gamma)^{15}\text{O}$  and  $^{12}\text{C}(\alpha, \gamma)^{16}\text{O}$  are from Formicola et al. (2004) and Kunz et al. (2002) respectively. Carbon and neon burning rates are taken from Caughlan & Fowler (1988). In our calculations, carbon burning is relevant only to the  $8 M_{\odot}$  model.

The equation of state used from the pre-main-sequence up to the beginning of the white dwarf cooling branch includes, for the low-density regime, partial ionization for hydrogen and helium compositions, radiation pressure and ionic contributions. For the high-density regime, partial electron degeneracy and Coulomb interactions are also included. For the white dwarf regime we adopt in regions of partial ionization an updated version of the equation of state of Magni & Mazzitelli (1979) that accounts for covolume, van der Waals, Coulomb and degeneracy effects. In regions where ionization is complete, non-relativistic or relativistic degeneracy, Coulomb and exchange effects, as well as Thomas-Fermi contributions at finite temperature are taken into account. The liquid and solid phases are also account for in the equation of state; however, the release of latent heat is not incorporated into the evolutionary models.

Neutrino emission rates are taken from Itoh et

al. (1989) with the exception of the plasma neutrino emission rates which are taken from Haft et al. (1994). Radiative opacities are from OPAL (Iglesias & Rogers 1996), complemented at low temperatures by those of Alexander & Ferguson (1994). Conductive opacities are from Hubbard & Lampe (1969); Itoh & Kohyama (1993). More details on LPCODE can be found in Althaus et al. (2003).

We take the initial abundance to be close to solar,  $X_{\text{init}} = 0.7055$ ,  $Y_{\text{init}} = 0.2755$ , and  $Z_{\text{init}} = 0.019$ . Convection is treated by means of the mixing length theory and our choice of the mixing length parameter  $\alpha_{\text{MLT}} = 1.8$  is representative of the outcome of an extensive calibration of solar models with varying assumptions on the input physics as well as the solar parameters carried out by Boothroyd & Sackmann (2003). By default, our calculations include a mild exponentially decaying diffusive overshoot at all formal convective boundaries (Herwig et al. 1997) with the adopted efficiency of  $f = 0.016$ . Overshooting is suppressed, however, during the main sequence evolution of models with  $M < 1.3M_{\odot}$ , as evidence suggests the absence of overshooting in such low-mass stars when they harbour a small convective core early in their main sequence (MS) evolution (Schlattl & Weiss 1999; Michaud et al. 2004). Microscopic diffusion is accounted for during the hot-white dwarf and white dwarf phases (see § 3 for definition of the different evolutionary phases considered in this work).

Two complementary mass loss prescriptions are used. During the evolution along the Red Giant Branch (RGB) and early Asymptotic Giant Branch (AGB) the Reimers (1975) law is adopted; while for the thermally-pulsing AGB (TP-AGB) phase, we use the semi-empirical mass loss prescription of Marigo et al. (1996), which relates the mass loss rate to the pulsational period of the star during the Mira phase and mimics the superwind phase observed in evolved AGB stars. The free parameter  $\eta$  in the Reimers prescription is set to 1 in all our calculations except for the  $1 M_{\odot}$  case. The precise choice of  $\eta$  for stars more massive than  $1.5 M_{\odot}$  is, however, of little consequence because these stars lose most of their mass on the TP-AGB phase, where the Marigo et al. mass loss prescription is applied. In the case of the  $1 M_{\odot}$  model its evolution along the RGB phase is slow enough

that a mass loss rate with  $\eta = 1$  removes all the hydrogen envelope before the helium-core is massive enough to ignite, thus evading the helium-core burning phase and leading to the formation of a helium-core white dwarf from a single progenitor. To avoid this non-canonical evolutionary channel, we force a lower mass loss rate by adopting  $\eta = 0.3$  for this model. An indirect check for the mass loss prescription is given by the final white dwarf mass.

We carry out evolutionary calculations from the phase of gravitational contraction to a pre-main sequence star continuously to a cooled white dwarf for stars to  $6M_{\odot}$ . For 7 and  $8M_{\odot}$ , however, we skip the latest phase of TP-AGB and the planetary nebula phase for technical reasons; we resume the calculation in the late planetary nebula phase.

### 3. Results

The physical quantities are presented in Table 1 for 1, 1.5, 1.8, and 2 to  $8M_{\odot}$  in one solar mass step, with each case divided into 7 phases (the  $0.8M_{\odot}$  model is given in Table 2 for the first three phases). A transition from a degenerate helium flash to gentle helium ignition takes place at around  $M \simeq 1.9M_{\odot}$  and physical features change rather abruptly across this mass; The two models with 1.5 and  $1.8M_{\odot}$ , together with the  $1M_{\odot}$  model allow us to study properties of stars that undergo helium flash. We use  $M$  to denote the initial mass of the star. Our definition for the 7 phases is:

(A) PMS (pre-main sequence) phase, which is approximately on the Hayashi track up to the minimum in the stellar luminosity that follows the reaccommodation of the CN abundances to their equilibrium values. This point is almost coincident with a local minimum in the gravitational binding energy of a star.

(B) MS (main sequence), up to the moment when the central mass fraction of hydrogen drops below 0.001. So, it includes gravitational contraction slightly after the turn-off from the main sequence.

(C) RGB (red giant branch). It includes subgiant evolution and ends on the RGB when the stellar luminosity reaches a maximum, coincident with helium ignition in the stellar core.

(D) He-core. From helium ignition up to the moment when the central helium mass fraction drops below 0.001.

(E) AGB (asymptotic giant branch). This phase includes early AGB (E-AGB) phase and the thermally pulsing phase (TP-AGB). Post-AGB evolution including the very first stages of white dwarf evolution (up to the point where neutrino cooling starts to dominate over photon radiation) is included in this phase for convenience (this evolutionary stage is very short and does not contribute significantly to the overall energetics of stars).

(F) Hot-WD (hot white dwarfs). Evolutionary stage during which energy loss by neutrino emission is more important than photon energy loss.

(G) WD (white dwarfs), up to the point down to  $L/L_{\odot} = -4.5$

The table contains the following fundamental evolutionary quantities: (1) age (in  $10^6$  yrs); (2) mass at the end of each step; (3) mean luminosity (averaged over the time); (4) mean radius; (5) mean effective temperature, and (6) mean surface gravity. (2)-(4) are in solar units.

Integrated energy output (in ergs) from each phase: (7)  $E_{\gamma}$ , energy emitted in photons (integrated bolometric photon luminosity), which is broken down into: (8)  $E_{\text{NIR}}$ , integrated luminosity in the infrared ( $\lambda > 10000\text{\AA}$ ); (9)  $E_{\text{opt}}$ , integrated luminosity in the optical band ( $3500 < \lambda < 10000\text{\AA}$ ); (10)  $E_{\text{UV}}$ , integrated luminosity in the UV ( $124 < \lambda < 3500\text{\AA}$ ); (11)  $E_X$ , integrated luminosity in X-rays ( $2 < \lambda < 124\text{\AA}$ ). Note that our numbers are only in thermal radiation with the assumption of the simple black body spectrum corresponding to the effective temperature. For extreme-UV and X-ray emission, non-thermal and magnetic-field related processes can be more important in reality; also, reprocessing of photons by dust is not considered; (12)  $E_{\text{H}}$ , energy released in photons from hydrogen burning; (13)  $E_{\text{He}}$ , the same but from helium burning. For the  $8M_{\odot}$  model the nuclear energy release from carbon burning,  $E_{\text{C}}$ , is listed after  $E_{\text{He}}$ . Energies in neutrinos are (14)  $E_{\nu}(\text{nucl})$ , neutrinos emitted in nuclear reactions; (15)  $E_{\nu}(\text{therm})$ , pair neutrinos emitted from thermal processes, such as Compton, plasmon decay,  $e^+e^-$  pair annihilation processes etc.

Global energies: (16)  $\Delta\Omega$ , change in gravitational binding energy. The binding energy is initially adjusted to zero, and  $\Delta\Omega$  is added at

each phase; then adding  $\Delta\Omega$  over the evolutionary phases gives the work required to dissipate stellar material to infinity; (17)  $\Delta U$ , change in internal energy.

Changes in the elemental abundance: (18)  $\Delta M(X)$ , net change in hydrogen mass by nuclear reactions; (19)  $\Delta M(Y)$ , net change in helium mass by nuclear reactions; (20)  $\Delta M(\text{CNO})$ , net change in the CNO elements by nuclear reactions; (21)  $\Delta M(\text{Ne} + \text{Mg})$ , net change in the Ne and Mg elements by nuclear reactions; all these quantities include the mass that is ejected by mass loss. (22)  $\delta M(X)$ , hydrogen mass lost by winds; (23)  $\delta M(Y)$ , helium mass lost by winds; (24)  $\delta M(\text{CNO})$ , CNO mass lost by winds; (25)  $\delta M(\text{Ne} + \text{Mg})$ , Ne and Mg mass lost by winds. Therefore, the helium mass in a star at the end of a particular evolutionary phase, for example, is

$$M(Y)_{\text{star}} = Y_{\text{init}}M + \sum \Delta M(Y) - \sum \delta M(Y), \quad (1)$$

where the summation extends from PMS up to the particular phase of interest.

Figure 1 shows the evolutionary track for each of our models (as indicated in each panel). Solid circles A–H indicate our definition of each phase, where A is our initial condition and B is the zero age main sequence and so on. H is the point at  $L/L_{\odot} = -4.5$ , the terminating point of our calculation. The table includes rich information. We summarise in what follows basic features from our preliminary reading, although much of the physics involved is that can be found in textbooks of stellar evolution.

### 3.1. Time-scales

The evolutionary time-scales are shown in Figure 2 for MS, RGB, He-core, AGB, Hot-WD and WD phases. For MS and RGB the  $0.8 M_{\odot}$  model is included. The results from the Geneva tracks are also plotted for MS and He-core. Good agreement is seen between Geneva calculations and ours (except for some difference for the He-core phase of the  $M = 1.8M_{\odot}$  model). The lifetime of MS varies as  $t_{\text{MS}} \sim M^{-3.5}$  for stars with fully radiative interiors ( $M < 1.3M_{\odot}$ ), changes to  $t_{\text{MS}} \sim M^{-3}$  in the range  $1.3M_{\odot} < M < 2.5M_{\odot}$  and becomes  $t_{\text{MS}} \sim M^{-2.3}$  for masses above  $3M_{\odot}$ .

The variation of lifetime of the He-core phase as a function of mass shows a glitch between 1.8

and  $2M_{\odot}$ . The  $1.8M_{\odot}$  model has a degenerate core and thus undergoes a helium flash but at flash ignition its helium core is somewhat smaller ( $0.432M_{\odot}$ ) than for less massive stars,  $0.462M_{\odot}$  and  $0.468M_{\odot}$  for the  $1.5M_{\odot}$  and  $1M_{\odot}$  models respectively. The maximum lifetime for the He-core phase takes place for the  $2M_{\odot}$  model, the least massive model to ignite helium under non-degenerate conditions; this model is the least luminous during helium-core burning. Across the glitch the lifetime becomes longer by a factor of 2, contrary to the general shortening trend of lifetime as the stellar mass increases. It is worth noting that stars just massive enough to have ignited helium under non-degenerate conditions are expected to populate a secondary, separated red clump (Girardi et al. 1998; Girardi 1999). The accurate mass range for which such a distinctive timescale for the He-core phase depends on details such as overshooting during the main sequence (for example, if overshooting is not included this mass range shifts towards higher mass values by  $\approx 0.3 - 0.4M_{\odot}$ ).

Good agreement with the Geneva tracks, despite many subtle differences in the treatment of overshooting and in nuclear reaction rates etc., endorses the reliability of the state-of-the-art stellar evolution calculations for the helium burning phase.

The lifetime of RGB varies as  $t_{\text{RGB}} \sim M^{-5.5}$  for  $M \leq 3M_{\odot}$  and  $\sim M^{-3.4}$  for higher masses. It is interesting to note that the lifetimes of AGB and RGB start agreeing for  $> 2M_{\odot}$ ; the two lifetimes almost coincide for  $M \geq 4M_{\odot}$ , despite the mean luminosity of AGB being higher by a factor of 3–4 than that of RGB for this mass range. The lifetime of AGB is much shorter than that of RGB for  $M < 2M_{\odot}$ . Early AGB evolution is much slower than that during the TP-AGB and dominates the overall AGB time-scales. Consequently, we expect the uncertainty in the mass loss rates during AGB evolution to have a negligible effect on the AGB time-scales.

The lifetime of He-core phase is nearly parallel to that of AGB for the entire mass range,  $1-8M_{\odot}$ , approximately one order of magnitude longer than the latter.

After a short phase of planetary nebulae, stars begin to cool and get on the white dwarf sequence. The lifetime during the Hot-WD phase, defined

as the time when neutrino cooling dominates over photon cooling, depends only weakly on the WD mass, ranging from  $1 \times 10^7$  yrs for the least massive WD model to about  $0.8 \times 10^7$  yrs for the most massive one. The integrated neutrino luminosities are in the range  $1.5 \pm 0.3 \times 10^{48}$  ergs for the whole WD mass range.

The lifetime of WD, which we define by the time needed from the epoch when photon cooling dominates over neutrino cooling to the epoch of  $\log L/L_\odot = -4.5$ , is almost constant ( $\sim t_{\text{WD}} = 7 - 8 \times 10^9$  yrs) for models with  $M_{\text{WD}} < 1M_\odot$  but decreases appreciably for more massive models, reaching about  $\sim t_{\text{WD}} = 4.8 \times 10^9$  yrs for the  $M_{\text{WD}} = 1.15M_\odot$  WD model. The integrated photon luminosity during the WD phase ranges between  $8 - 15 \times 10^{47}$  ergs. Note that contribution from nuclear burning to the energy budget of the WD decreases monotonically with increasing WD mass. It is about 22% for the  $1M_\odot$  ( $0.52M_\odot$  WD mass), it becomes negligible (about 0.1%) for the  $0.79M_\odot$  and 0.001% for the  $8M_\odot$  ( $1.15M_\odot$  WD mass).

### 3.2. Stellar structure parameters

The stellar radii may expand by up to a factor of 2 during the evolution on the main sequence; so in what follows we consider time-averaged values over the MS. Gravitational binding energies are also time averages. The mean radii are plotted in Figure 3 (a) for the main sequence stars as a function of mass. See Table 3 for numbers.

The dependence of stellar radii on the stellar mass is approximated as

$$\log_{10} R = \begin{cases} 0.020 + 1.40 \log M & \text{for } M \leq 1.5 \\ 0.185 + 0.55 \log M & \text{for } M \geq 1.5 \end{cases} \quad (2)$$

in solar units.

We define (FP) the structure constant  $K$ , as

$$\Omega_g = -K \frac{GM^2}{R}, \quad (3)$$

which is also shown in Figure 3 (b). On the main sequence, the total average gravitational binding energy varies by a factor of 15 in the mass range from 1 to  $8M_\odot$ , while  $K$  only varies by a factor up

to 1.5.  $K$  is described approximately by

$$\log_{10} K = \begin{cases} 0.21 + 0.8 \log M & \text{for } M \leq 1.5 \\ 0.4 - 0.15 \log M & \text{for } M \geq 1.5. \end{cases} \quad (4)$$

We remark that gravitational contraction continues in the MS for stars with radiative cores ( $M \leq 1.3M_\odot$ ) while for more massive stars, i.e. those with a convective core, the modulus of the gravitational energy slowly decreases with the MS evolution.

The similar quantities averaged over the WD phase are shown in Figure 3 (c) and (d) as a function of the final white dwarf mass. The models shown correspond to 10 models of initial 1 to  $8M_\odot$ . The gap between the  $0.6M_\odot$  white dwarf model ( $3M_\odot$  progenitor) and the  $0.79M_\odot$  model ( $4M_\odot$  progenitor) is commented on in § 3.5. Panel (d) shows that the structure factor  $K$  (for which  $M$  is replaced with the white dwarf mass  $m_f$ ) is basically constant,  $K = 0.95 \pm 0.02$ , with a weakly increasing trend: the gravitational energy changes by a factor larger than 5 across this mass range.

For other evolutionary phases  $K$  varies wildly with the mass, meaning that the density profile of stars are strongly mass-dependent. Table 3 gives the mean  $R$  and  $K$  for the phases of MS, RGB, He-core and WD, where  $K$  is defined by equation (3) with  $M$  replaced by the mass in the relevant phase.

### 3.3. Energy output

Figure 4 shows the photon energy output integrated over the time of each phase (and the sum) as a function of stellar mass in logarithmic scales. This shows that it is enough to consider MS, RGB, He-core and AGB for global energetics. The total energy of radiation increases from  $E_{\text{photon}} = 5 \times 10^{51}$  for the  $1M_\odot$  model to  $20 \times 10^{51}$  for  $8M_\odot$ .

The energy output from PMS is approximately 1/160 that from MS. Approximately 3/4 of its energy is derived from gravitational contraction. Optical emission is intrinsically more important than IR (we are ignoring here the dust around those nascent stars). The energy emitted in the IR band is 30 – 40% of the total energy for  $1M_\odot$ , but its importance decreases with increasing  $M$ .

Now we pay some attention to energies produced in the four major phases. In three panels of

Figure 5 we present the energy output in different arrangements to stress various aspects of energy production. We show the relative importance of energy output in each phase of the evolution in Panel (a). At low mass  $M < 1.5M_{\odot}$  MS gives only a subdominant contributions, 20–30% the total, and RGB is by far the important energy source. The importance of RGB phase, however, drops sharply by  $M = 2M_{\odot}$ , and MS becomes the dominant energy source. The energy fraction of RGB drops from 55% at  $1M_{\odot}$  to 5% at  $2M_{\odot}$ , and for  $M \geq 3M_{\odot}$  it becomes a negligible amount (<2%). This is understood by the following consideration: for  $M < 2M_{\odot}$  models the helium core mass at the end of the main sequence phase is small and substantial hydrogen shell burning is needed to prepare the helium core of  $m_c \approx 0.47M_{\odot}$ , the critical mass for helium ignition under the degenerate condition. This contrasts to the case for  $M > 2M_{\odot}$ , for which the star leaves the main sequence with a substantial helium core mass, and there is no need to increase the core mass substantially before helium ignition; the time scale of RGB is more importantly governed by the Kelvin-Helmholtz contraction time-scale, during which the temperature rises to  $10^8\text{K}$ . This brings a drastic drop of the energy emitted in the RGB phase across the transition mass.

He-core burning phase and AGB each produces  $1/2$ – $1/3$  the amount of energy MS produces. The relative importance of AGB shows a gradual decline towards higher masses for  $M \geq 2M_{\odot}$ . We note that, while AGB is not bolometrically important, it becomes dominant over the other phases for  $M \approx (2 - 3)M_{\odot}$  stars, if one is concerned with the near infrared light. The synthetic  $K$  band light over stellar populations is thus disturbed strongly by AGB stars (see Bruzual & Charlot 2003). For lower mass stars the near infrared light is dominated by RGB and for higher mass by He-core stars.

It would also be useful to see the energy generation from a different view. Panel (b) shows the energy output per initial mass,  $E_{\gamma}/M$ , i.e., the efficiency as an energy producing engine. The overall efficiency drops sharply from 1 to  $3M_{\odot}$ , and varies only slowly for  $M > 3M_{\odot}$ . The breakdown to the phases shows that the efficiency of the MS phase increases, but only gradually from  $1M_{\odot}$  to higher mass. This represents what is often char-

acterised as “when 10% of hydrogen is consumed, MS evolves off the main sequence”. In fact, the consumed hydrogen is 9.7% of the total mass at  $1M_{\odot}$ . It increases to 17% at  $8M_{\odot}$ . We note that this statement is *not* valid for lower mass stars: a kink is observed in  $E_{\gamma}/M$  at  $1M_{\odot}$ , which means the efficiency turning to increase to lower mass. We confirmed in separate MS calculations with a finer mass mesh that this kink in fact takes place at  $1.3 M_{\odot}$  where the core changes from radiative to convective; there is actually a small jump at this mass (not manifest in the figure) above which we assumed convective overshooting. Even if we do not take overshooting for  $1.3 M \geq M_{\odot}$ , the kink still exists at the same mass but without a jump. For masses smaller than  $1 M_{\odot}$ , what is constant is the integrated energy output  $E_{\gamma}$  and not  $E_{\gamma}/M$  (see Figure 4).

For stars in which helium flash takes place ( $M \leq 1.8M_{\odot}$ ), the integrated energy output from RGB stays at constant at  $3 \times 10^{51}$  ergs for  $M \lesssim 1M_{\odot}$  and decreases rather weakly to the maximum mass. This is due to the fact that the helium-core mass when the flash ignites is almost independent of the initial mass of the star for  $M \lesssim 1M_{\odot}$  and it weakly decreases as the initial mass increases. Therefore  $E_{\gamma}/M$  decreases somewhat faster than  $1/M$ . It drops rapidly as the degeneracy is lost in the core. The energy output is nearly mass independent for high mass stars with non-degenerate cores: the luminosity and the lifetime nearly compensate.

For the helium burning phase (He-core),  $E_{\gamma}/M$  is nearly constant for all masses at  $0.5 \times 10^{51}$  ergs per solar mass. It gives 20% of total energy for  $M > 2M_{\odot}$ .

Figure 5(c) shows the fractional energy production from helium burning and its subcomponent from the He-core phase. The fractional total energy production from helium burning decreases gently with the mass: it is 15% for low mass ( $M \leq 2M_{\odot}$ ) stars and 10% for high mass stars. In helium core burning phase of  $1M_{\odot}$  stars, helium burning produces 1.8 time more energy than hydrogen burning. At  $2 M_{\odot}$  this factor drops to 0.3 and starts increasing again to 0.5-0.6 for  $M > 3M_{\odot}$ . In the AGB phase helium burning is the most important energy source except for  $2 - 3M_{\odot}$  where H burning energy is larger. It is worth noting that the dominant contribution to

helium burning during the AGB phase comes from the E-AGB.

The energetic contribution of the most advanced evolutionary stages, after the track of AGB stars reaches the maximum luminosity, is insignificant ( $< 0.1\%$ ), including that of the long white dwarf phase.

### 3.4. Neutrino production

Figure 6 shows the fraction of energy in neutrinos through the life of stars. The two open symbols represent neutrinos produced by nuclear reactions and those of thermal origin. The latter stay insignificant for the mass range that concerns us; they begin to rise only at  $8M_{\odot}$ . The gradual increase of the neutrino energy fraction from 1 to  $3M_{\odot}$  represents an increasing importance of the later part of the  $pp$  chain and then the dominance of the CNO cycle. Hydrogen shell burning is always dominated by the CNO cycle. We expect 6.4% of energy fractions from beta decay of  $^{13}\text{N}$  and  $^{15}\text{O}$  for the CN cycle. Neutrinos from NO cycle, originating in the beta decay of  $^{17}\text{F}$ , have higher energy, but because the branching between CN and the NO cycles is almost independent of temperature, they are always a minor contributor. The nuclear neutrino energy fraction actually seen in Figure 6 is approximately 10% less than the value quoted above because  $L_{\gamma}$  includes the energy production by helium burning, which produces a negligible amount of neutrinos (helium burning is an important source of neutrinos only at the helium flash, see Serenelli & Fukugita 2005).

The Hot-WD and WD phases give only insignificant contributions for neutrinos at several times  $10^{48}$  erg. The dominant neutrino production is from plasmon decay. The integrated neutrino energy is comparable to that of photons for stars with  $M \leq 3M_{\odot}$ . For high mass stars energies carried away by neutrinos win but only by a factor of 2.

### 3.5. Mass loss and remnants

After some nuclear reprocessing, stars return part of their stellar matter to the interstellar medium. The mass lost by winds in our models is shown in Figure 7, where the total, hydrogen, helium and total metal masses lost per unit initial mass are shown. To help understanding the

amount of matter that underwent nuclear reprocessing, the equivalent amount that would be expected if reprocessing of the stellar matter would be switched off is shown by dotted curves. The difference between the solid and dotted curves is the effect of nuclear reprocessing in stars. In our calculation,  $> 95\%$  of mass is retained up to the beginning of AGB for  $M \geq 2M_{\odot}$  stars. For  $1M_{\odot}$  stars 25% of mass is already lost in the RGB phase and another 25% (relative to initial mass) in the AGB phase. More than 80% of mass is lost by winds for  $M > 3M_{\odot}$ .

The composition of the lost mass depends appreciably on the stellar mass. The hydrogen and helium abundances are mostly determined by the increasing efficiency with mass of the first dredge up event for stars with masses below  $\sim 4M_{\odot}$  and by both the first and second dredge up for masses above this value. While these events alter the distribution of the CNO elements (nitrogen is enhanced while carbon and oxygen are depleted), the total metallicity  $Z$  of the stellar envelope is hardly affected. The increase in the metallicity of the lost mass occurs during the third dredge up, where material partially processed by helium-shell burning (mostly carbon and to a lesser extent oxygen) is mixed into the envelope during the TP-AGB phase. The efficiency of the third dredge up in our models is most noticeable for stars with masses below  $\sim 4M_{\odot}$  as can be seen in Figure 7. For the range of masses considered in this work, the added contribution of neon, magnesium and heavier elements to the envelope metallicity remains almost constant and equal to its initial value.

The remaining mass forms a white dwarf. The initial mass ( $M$ ) - final mass ( $m_f$ ) relation (IFMR) gives a check for the calculation of the mass loss. Figure 8 shows the IFMR, with Weidemann (2000)'s semi-empirical relation added for comparison. They agree to within 5%, except at the initial mass  $3M_{\odot}$ , for which our calculation gives a white dwarf mass 15% lower than Weidemann's value. The "anchor point" of Weidemann,  $m_f = 0.8M_{\odot}$  at  $M = 4M_{\odot}$ , is met nearly exactly in our calculation, which gives  $m_f = 0.79M_{\odot}$ .

We may ascribe the particularly small mass,  $m_f = 0.6M_{\odot}$ , at  $M = 3M_{\odot}$  to convective overshooting during the TP-AGB phase that is effective at the inner front of the helium convective shell and pushes the helium shell inwards during a

thermal pulse, effectively preventing an increase in size of the CO-core. If overshooting is suppressed or if its efficiency is limited at this specific convective boundary, then the final mass for our  $M = 3M_{\odot}$  could be about  $0.68M_{\odot}$  in agreement with Weideman's value.<sup>1</sup> We note that theoretical models used by Weidemann (2000) to derive his IFMR involve either synthetic AGB evolution (e.g. Girardi et al. 2000) or full stellar evolution models that do not include overshooting (Blöcker 1995) and this prevents a detailed comparison with our results. While we do not fully understand the origin of the discrepancy, we believe that the inclusion of overshooting beyond the formal Schwarzschild convective boundaries in the helium convective shell lies at its roots. The current observational data (e.g., see, Claver et al. 2001) show too large a scatter and we cannot distinguish between the two cases. This effect of overshooting becomes weak already at  $M = 4M_{\odot}$  and negligible towards the high mass end covered by our models.

In Figure 8 a line  $m_f = 0.085M + 0.44$ , which is close to the empirical mass relation of Claver et al. (2001), is drawn for a reference; it describes the  $M - m_f$  relation reasonably well, again except for the dip at  $M = 3M_{\odot}$ . At the high mass end, our  $M = 8M_{\odot}$  model leads to a  $m_f = 1.15M_{\odot}$  WD with a ONe core, very close to the minimum mass for core-collapse that will likely be about  $9M_{\odot}$ . We note that our white dwarf masses are smaller than that of Girardi et al. (2000) for a given initial mass. Their  $m_f$  reaches  $1.15M_{\odot}$  for  $M = 5M_{\odot}$ , thus the onset of core collapse supernovae takes place at  $M \approx 6M_{\odot}$ . We note, however, that the synthetic AGB calculations employed by Girardi et al. (2000) predict a substantial growth of the hydrogen depleted core during TP-AGB evolution, in contradiction with full evolutionary models of TP-AGB stars which, particularly for stellar masses  $\gtrsim 4M_{\odot}$ , predict a very small or even negligible increase in the core size (i.e. this paper, Blöcker et al. 2000; Herwig 2000).

<sup>1</sup>It should be noted, however, that an amount of overshooting operating at the inner boundary of the helium convective shell similar to the one adopted in this paper (or some other mechanism providing extra mixing) is necessary to explain the surface abundances of PG-1159 stars Herwig et al. (1999).

#### 4. Summary

The central result of this paper is Table 1, which documents products of stars integrated over time for each phase. We consider stars from 1 to  $8M_{\odot}$ . This can be used to link baryon mass locked into stars to extragalactic background light, and also to predict chemical enrichment. The table also tells us the relative importance of each phase for the light emitted by stars. Some discussion is made to understand the trend of numbers we present in the table.

When the numbers in the table are integrated over the initial mass function, they give the output of photon and neutrino energies from respective phases of stellar evolution and helium and CNO enrichment per given mass of cooled baryons, although the calculation still must be supplemented by a similar table for more massive stars. When they are further integrated over star formation history, we can estimate differential contributions to the energetics of the galaxies and Universe. Such procedures will make the work similar to that of population synthesis model, the most recent example of which is Bruzual & Charlot (2003). The difference lies in the fact that the latter is specifically oriented for the calculation of the detailed spectral output of the stellar radiation, while our aim is to calculate all outputs in a gross form from the stellar population divided into each stage.

We would like to thank Jim Peebles for useful discussions from time to time. AMS is supported by the NSF (grant PHY-0503684), the W. M. Keck Foundation through a grant-in-aid to the Institute for Advanced Study and by the Association of Members of the Institute for Advanced Study. MF is supported by the Monell Foundation at the Institute for Advanced Study, and by Grant-in-Aid of the Ministry of Education at the University of Tokyo.

#### REFERENCES

- Alexander, D. R., & Ferguson, J. W., 1994, *ApJ*, 437, 879
- Althaus, L. G., Serenelli, A. M., Córscico, A. H., & Montgomery, M. H. 2003, *A&A*, 404, 593
- Angulo, C. et al. 1999, *Nuc. Phys. A*, 656, 3



- Blöcker, T., 1995, *A&A*, 297, 727
- Blöcker, T., Herwig, F., & Driebe, T., 2000, *Mem. Soc. Astron. Ital.*, 71, 711
- Boothroyd, A. I., & Sackmann, I.-J., 2003, *ApJ*, 583, 1004
- Bruzual, G., & Charlot, S. 2003, *MNRAS*, 344, 1000
- Caughlan, G. R., & Fowler, W. A., 1988, *Atom. Data and Nuc. Data*, 40, 283
- Charbonnel, C., Meynet, G., Maeder, A., & Schaerer, D. 1996, *A&AS*, 115, 339
- Claver, C. F., Liebert, J., Bergeron, P., & Koester, D. 2001, *ApJ*, 563, 987
- Formicola, A. et al., 2004, *Phys. Lett. B*, 591, 61
- Fukugita, M., & Peebles, P. J. E. 2004, *ApJ*, 616, 643
- Girardi, L., Groenewegen, M. A. T., Weiss, A., & Salaris, M. 1998, *MNRAS*, 301, 149
- Girardi, L. 1999, *MNRAS*, 308, 818
- Girardi, L., Bressan, A., Bertelli, G., & Chiosi, C. 2000, *A&AS*, 141, 371
- Haft, M., Raffelt, G., & Weiss, A. 1994, *ApJ*, 425, 222
- Herwig, F., Blöcker, T., Schönberner, D., & El Eid, M. 1997, *A&A*, 324, L81
- Herwig, F., Blöcker, T., Langer, N., & Driebe, T., 1999, *A&A*, 349, L5
- Herwig, F., 2000, *A&A*, 360, 952
- Hubbard, W. B., & Lampe, M., 1969, *ApJS*, 18, 297
- Iglesias, C. A., & Rogers, F. J., 1996, *ApJ*, 464, 943
- Itoh, N., Adachi, T., Nakagawa, M., Kohyama, Y., & Munakata, H. 1990, *ApJ*, 339, 354
- Itoh, N., & Kohyama, Y., 1993, *ApJ*, 404, 268
- Kunz, R., Fey, M., Jaeger, M., Mayer, A., Hammer, J. W., Staudt, G., Harissopulos, S., & Paradellis, T., 2002, *ApJ*, 567, 643
- Magni, G., & Mazzitelli, I. 1979, *A&A*, 72, 134
- Marigo, P., Bressan, A., & Chiosi, C. 1996, *A&A*, 313, 545
- Michaud, G., Richard, O., Richer, J., & Vandenberg, D. A. 2004, *ApJ*, 606, 452
- Reimers, D. 1975, *Memoires of the Societe Royale des Sciences de Liege*, 8, 369
- Schaller, G., Schaerer, D., Meynet, G., & Maeder, A. 1992, *A&AS*, 96, 269
- Schlattl, H., & Weiss, A. 1999, *A&A*, 347, 272
- Serenelli, A. M., & Fukugita, M. 2005, *ApJ*, 632, L33
- Weidemann, V. 2000, *A&A*, 363, 647

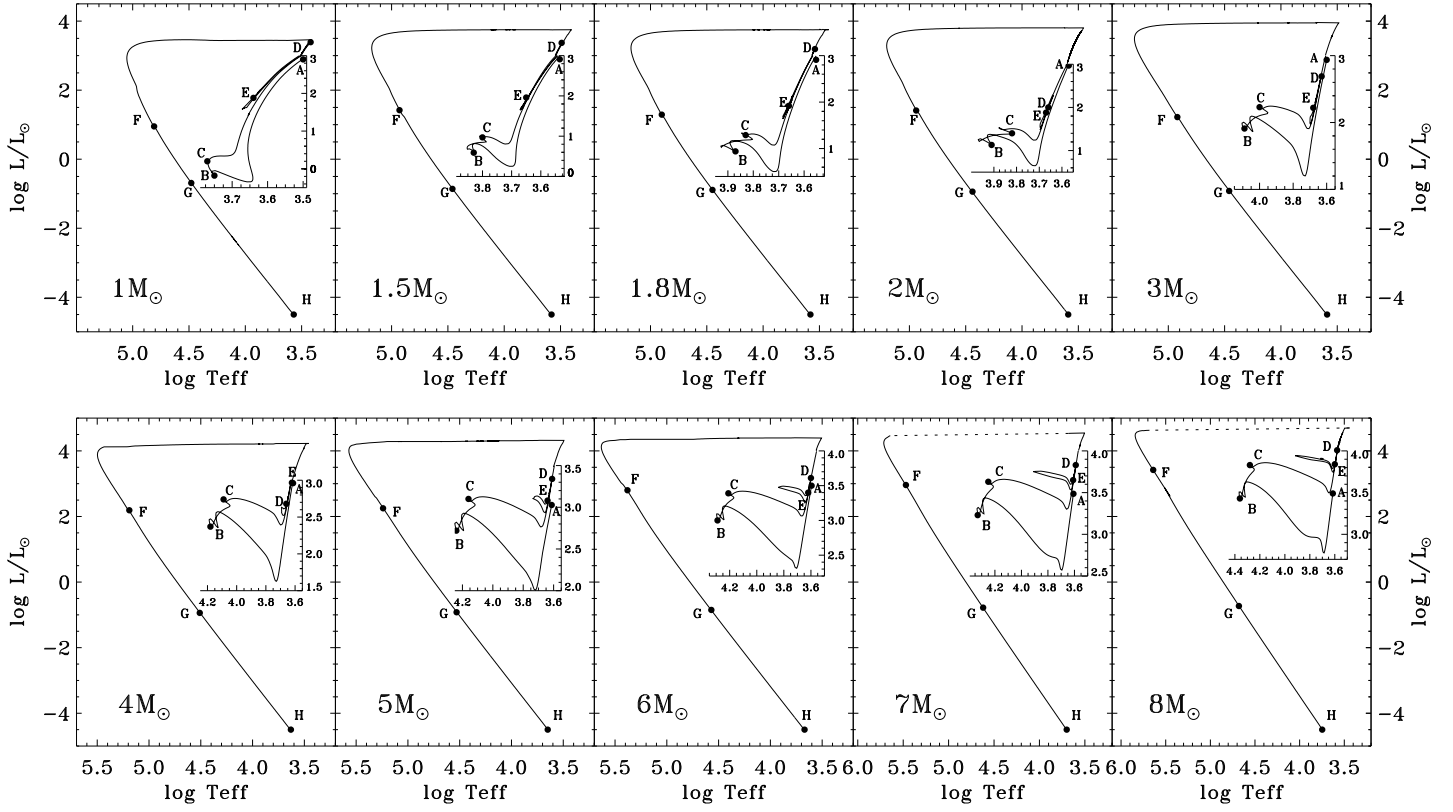


Fig. 1.— Evolutionary tracks for our models. A to H stand for the points for the six phases defined in the text. In particular, B-C is the main sequence and D-E is helium core burning. The dotted line segment for the 7 and 8 $M_{\odot}$  models is the part we skipped calculations as described in the text.

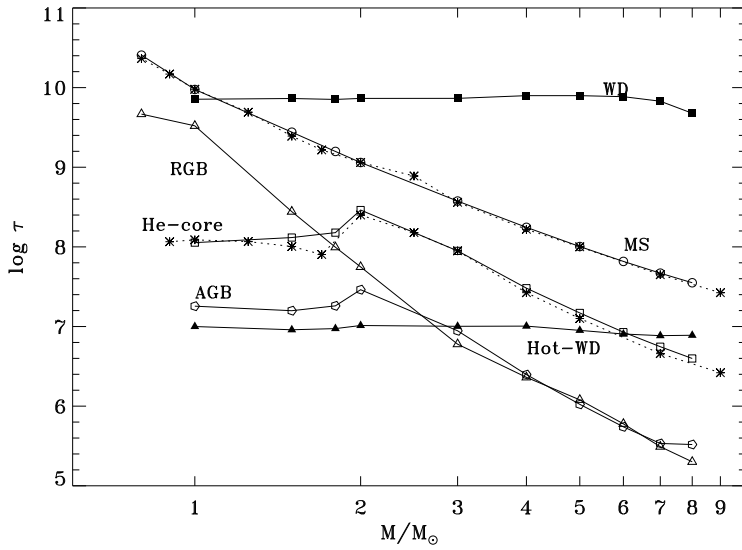


Fig. 2.— Lifetime of each phase (indicated by the legend) as a function of mass. For the main sequence and the RGB phase the  $0.8M_{\odot}$  model is added. Asterisks and dotted lines are the lifetime from the Geneva track.

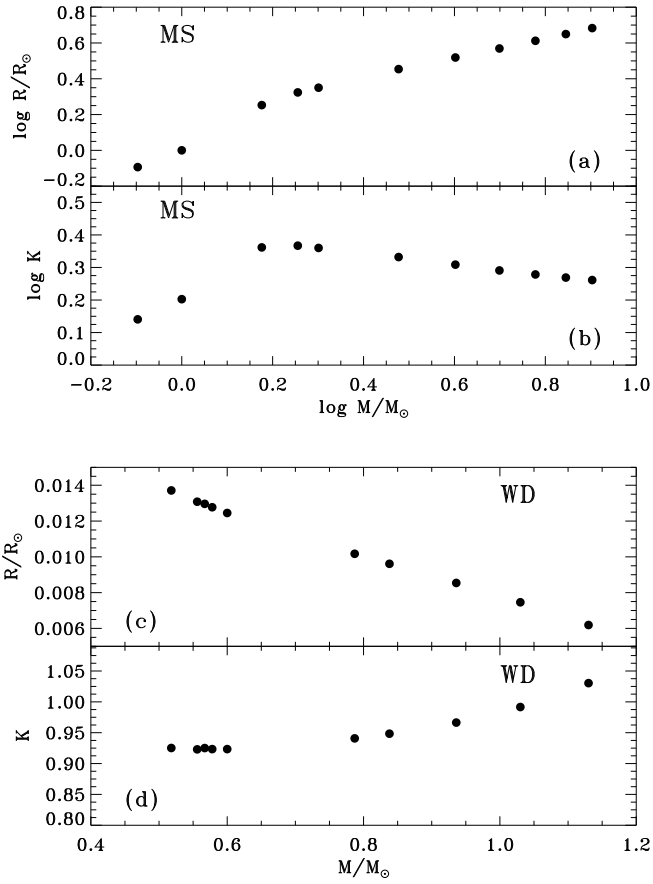


Fig. 3.— Stellar radius and the structure constant as a function of the mass. Panels (a) and (b) are for main sequence stars (in logarithmic scales), and (c) and (d) for white dwarfs (in linear scales).

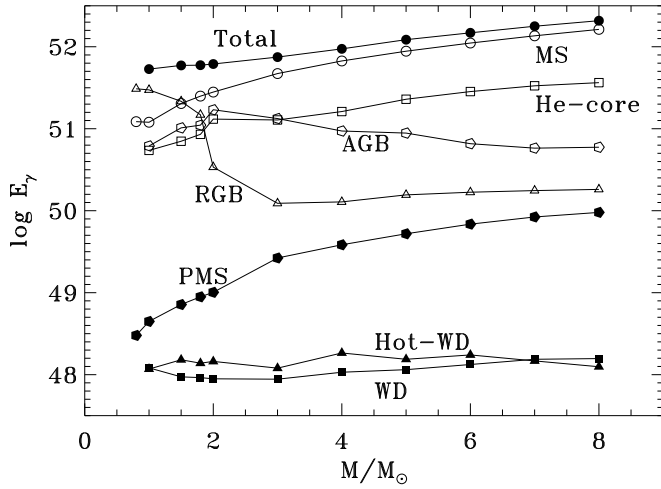


Fig. 4.— Photon energy output in the life of stars and the breakdown into each phases (indicated by the legend) plotted as a function of stellar mass.  $E_\gamma$  is in units of ergs.

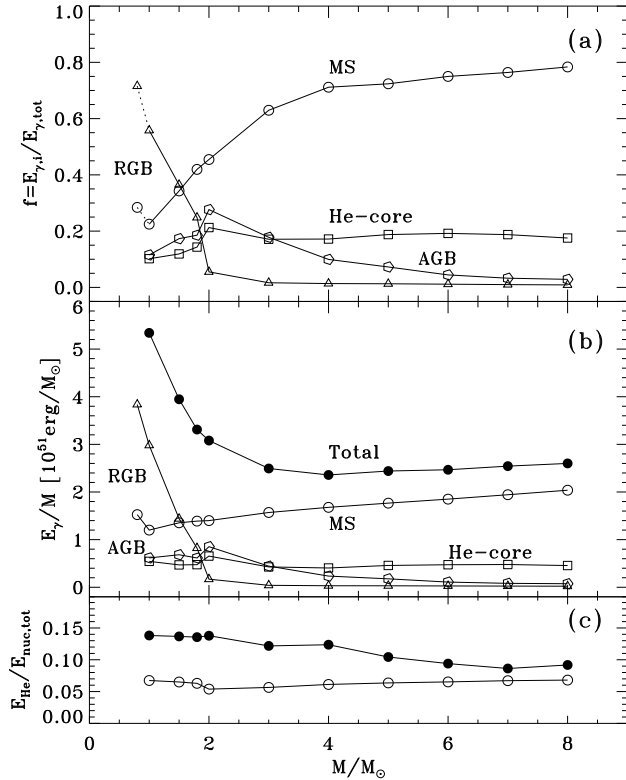


Fig. 5.— (a) Fractional photon energy output from the four major phases. The  $0.8M_\odot$  model is added for the MS and RGB phases. (b) Photon energy production per initial stellar mass. (c) Fraction of the photon energy production from helium burning. The open symbols are the contribution from the helium core burning phase.

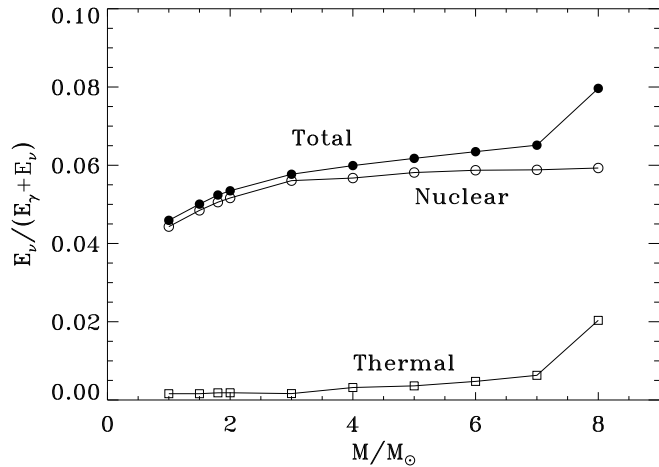


Fig. 6.— Fraction of neutrino energy integrated over the entire life of stars. The open circles are neutrino energy from nuclear reaction processes and the open squares are from the thermal pair-neutrino production.

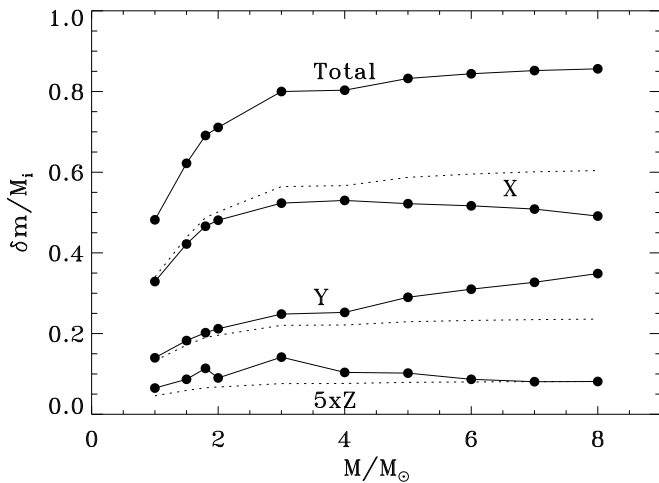


Fig. 7.— Fractional mass loss of stars (relative to the initial stellar mass). X, Y and Z are breakdown into hydrogen, helium and heavy elements (scaled up by a factor of 5). The dotted curves are the equivalent amount when the stellar matter would not be reprocessed by nuclear reactions.

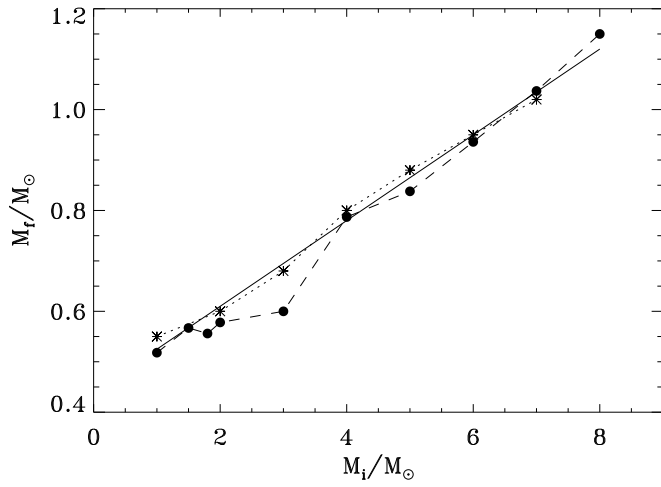


Fig. 8.— Initial-final mass relation. Solid circles stand for our calculation. Asterisks are the semi-empirical relation of Weidemann. The solid line is the relation  $m_f = 0.085M + 0.44$ .

TABLE 1  
EVOLUTIONARY CHARACTERISTICS OF LOW AND INTERMEDIATE MASS STARS.

	PMS	MS	RGB	He-core	AGB	Hot-WD	WD	Total
$1M_{\odot}$								
Age	46.5	9477	12789	12902	12920	12930	20074	—
Mass	1.0	0.995	0.751	0.744	0.518	0.518	0.518	—
$\log L/L_{\odot}$	-0.15	0.00	0.91	1.60	2.47	0.28	-2.85	—
$R$	1.09	1.00	2.60	9.74	37.3	0.0191	0.0137	—
$\log T_{\text{eff}}$	3.71	3.76	3.74	3.67	3.60	4.67	3.77	—
$\log g_{\text{sup}}$	4.41	4.45	4.05	2.34	1.51	7.60	7.88	—
$E_{\gamma}$	4.46E+48	1.20E+51	2.98E+51	5.44E+50	6.15E+50	1.17E+48	1.21E+48	5.34E+51
$E_{\text{NIR}}$	1.59E+48	3.37E+50	1.55E+51	2.25E+50	3.65E+50	1.30E+45	5.38E+46	2.47E+51
$E_{\text{Opt}}$	2.68E+48	7.76E+50	1.38E+51	3.07E+50	2.34E+50	2.30E+46	2.71E+47	2.70E+51
$E_{\text{UV}}$	1.88E+47	8.48E+49	5.69E+49	1.22E+49	1.66E+49	1.14E+48	8.87E+47	1.72E+50
$E_{\text{X}}$	—	—	—	—	9.91E+45	2.10E+42	—	9.91E+45
$E_{\text{H}}$	1.47E+48	1.20E+51	2.97E+51	1.96E+50	2.12E+50	3.29E+47	2.65E+47	4.59E+51
$E_{\text{He}}$	—	—	1.69E+47	3.59E+50	3.76E+50	2.86E+45	—	7.36E+50
$E_{\nu}(\text{nucl})$	4.28E+46	3.20E+49	1.88E+50	1.31E+49	1.51E+49	2.08E+46	7.29E+45	2.48E+50
$E_{\nu}(\text{ther})$	—	1.42E+43	2.62E+47	7.13E+47	6.48E+48	1.32E+48	3.77E+47	9.15E+48
$\Delta\Omega$	-5.97E+48	-2.35E+47	-3.47E+49	2.48E+49	-4.53E+49	-5.03E+48	-3.00E+48	-6.95E+49
$\Delta U$	2.98E+48	1.24E+47	1.82E+49	-1.32E+49	2.40E+49	2.88E+48	1.68E+48	3.66E+49
$\Delta M(\text{X})$	-1.66E-04	-9.66E-02	-2.40E-01	-1.64E-02	-1.80E-02	-2.91E-05	-2.43E-05	-3.72E-01
$\Delta M(\text{Y})$	1.57E-04	9.65E-02	2.40E-01	-2.32E-01	-2.25E-01	2.61E-05	2.23E-05	-1.20E-01
$\Delta M(\text{CNO})$	8.67E-06	1.40E-04	-2.54E-04	2.43E-01	2.38E-01	3.00E-06	—	4.81E-01
$\Delta M(\text{Ne+Mg})$	—	—	—	5.37E-03	4.73E-03	—	—	1.01E-02
$\delta(\text{X})$	1.56E-05	3.32E-03	1.70E-01	4.89E-03	1.54E-01	—	—	3.29E-01
$\delta(\text{Y})$	6.07E-06	1.30E-03	7.06E-02	2.12E-03	6.68E-02	—	—	1.40E-01
$\delta(\text{CNO})$	3.05E-07	6.51E-05	3.38E-03	9.89E-05	3.13E-03	—	—	6.61E-03
$\delta(\text{Ne+Mg})$	5.19E-08	1.11E-05	5.75E-04	1.68E-05	5.31E-04	—	—	1.12E-03



TABLE 1—*Continued*

	PMS	MS	RGB	He-core	AGB	Hot-WD	WD	Total
<hr/> 1.5M <sub>⊙</sub> <hr/>								
Age	15.0	2756	3033	3163.8	3179.8	3188.9	10491	
Mass	1.5	1.5	1.197	1.174	0.567	0.567	0.567	
log $L/L_{\odot}$	0.60	0.79	1.81	1.69	2.73	0.15	-2.97	
$R$	2.04	1.79	10.0	10.8	49.9	0.0164	0.0130	
log $T_{\text{eff}}$	3.75	3.83	3.70	3.67	3.60	4.63	3.78	
log $g_{\text{sup}}$	4.08	4.14	3.31	2.45	1.66	7.77	7.97	—
$E_{\gamma}$	7.17E+48	2.03E+51	2.16E+51	7.04E+50	1.02E+51	1.52E+48	9.42E+47	5.92E+51
$E_{\text{NIR}}$	2.44E+48	4.18E+50	1.13E+51	2.91E+50	6.72E+50	1.59E+45	5.08E+46	2.52E+51
$E_{\text{Opt}}$	4.24E+48	1.34E+51	9.99E+50	3.98E+50	3.46E+50	2.77E+46	2.53E+47	3.08E+51
$E_{\text{UV}}$	4.94E+47	2.75E+50	2.68E+49	1.56E+49	8.43E+48	1.49E+48	6.39E+47	3.34E+50
$E_{\text{X}}$	—	—	—	—	2.81E+46	3.46E+43	—	2.81E+46
$E_{\text{H}}$	1.76E+48	2.03E+51	2.15E+51	3.30E+50	5.57E+50	2.88E+47	1.21E+47	5.07E+51
$E_{\text{He}}$	—	—	1.75E+47	3.82E+50	4.21E+50	3.26E+45	—	8.03E+50
$E_{\nu}(\text{nucl})$	7.62E+46	9.77E+49	1.43E+50	2.28E+49	3.77E+49	1.84E+46	3.27E+45	3.02E+50
$E_{\nu}(\text{ther})$	—	2.77E+43	2.72E+47	8.82E+47	7.53E+48	2.09E+48	1.85E+47	1.10E+49
$\Delta\Omega$	-1.08E+49	6.72E+47	-2.93E+49	2.25E+49	-5.99E+49	-7.94E+48	-2.36E+48	-8.71E+49
$\Delta U$	5.39E+48	-3.05E+47	1.48E+49	-1.15E+49	3.08E+49	4.63E+48	1.36E+48	4.52E+49
$\Delta M(\text{X})$	-1.81E-04	-1.67E-01	-1.78E-01	-2.63E-02	-4.64E-02	-2.54E-05	-1.13E-05	-4.18E-01
$\Delta M(\text{Y})$	1.67E-04	1.67E-01	1.78E-01	-2.33E-01	-2.40E-01	2.48E-06	1.25E-05	-1.27E-01
$\Delta M(\text{CNO})$	1.30E-04	1.87E-05	-1.12E-04	2.53E-01	2.80E-01	6.74E-07	—	5.33E-01
$\Delta M(\text{Ne+Mg})$	—	—	—	5.62E-03	5.62E-03	—	—	1.12E-02
$\delta(\text{X})$	—	—	2.08E-01	1.60E-02	4.16E-01	—	—	6.40E-01
$\delta(\text{Y})$	—	—	8.88E-02	6.86E-03	1.78E-01	—	—	2.74E-01
$\delta(\text{CNO})$	—	—	4.22E-03	3.25E-04	8.46E-03	—	—	1.30E-02
$\delta(\text{Ne+Mg})$	—	—	7.12E-04	5.48E-05	1.43E-03	—	—	2.20E-03

TABLE 1—*Continued*

	PMS	MS	RGB	He-core	AGB	Hot-WD	WD	Total
<hr/> 1.8M <sub>⊙</sub> <hr/>								
Age	9.54	1579	1678	1829	1847.4	1856.6	8964	
Mass	1.8	1.8	1.665	1.647	0.556	0.556	0.556	
log $L/L_{\odot}$	0.92	1.12	2.09	1.69	2.69	0.10	-2.97	
$R$	2.38	2.11	15.6	10.1	42.7	0.0165	0.0131	
log $T_{\text{eff}}$	3.81	3.89	3.69	3.68	3.62	4.62	3.78	
log $g_{\text{sup}}$	4.04	4.11	3.08	2.65	1.90	7.75	7.95	—
$E_{\gamma}$	8.90E+48	2.50E+51	1.48E+51	8.54E+50	1.10E+51	1.38E+48	9.16E+47	5.96E+51
$E_{\text{NIR}}$	3.25E+48	4.09E+50	7.39E+50	3.35E+50	6.84E+50	1.60E+45	5.00E+46	2.17E+51
$E_{\text{Opt}}$	4.91E+48	1.59E+51	7.21E+50	4.95E+50	4.12E+50	2.76E+46	2.48E+47	3.23E+51
$E_{\text{UV}}$	7.40E+47	4.99E+50	1.98E+49	2.33E+49	1.01E+49	1.35E+48	6.19E+47	5.57E+50
$E_{\text{X}}$	—	—	—	—	2.42E+46	1.58E+43	—	2.42E+46
$E_{\text{H}}$	1.98E+48	2.51E+51	1.47E+51	4.91E+50	6.49E+50	2.59E+47	1.14E+47	5.12E+51
$E_{\text{He}}$	—	—	1.40E+47	3.73E+50	4.30E+50	2.02E+45	—	8.03E+50
$E_{\nu}(\text{nucl})$	9.76E+46	1.43E+50	9.83E+49	3.28E+49	4.31E+49	1.66E+46	3.08E+45	3.18E+50
$E_{\nu}(\text{ther})$	—	3.11E+43	3.11E+47	8.92E+47	7.55E+48	1.87E+48	1.89E+47	1.08E+49
$\Delta\Omega$	-1.39E+49	1.35E+48	-2.01E+49	1.63E+49	-5.72E+49	-7.07E+48	-2.30E+48	-8.30E+49
$\Delta U$	6.93E+48	-6.36E+47	1.02E+49	-6.33E+48	2.97E+49	4.09E+48	1.31E+48	4.16E+49
$\Delta M(\text{X})$	-2.02E-04	-2.10E-01	-1.22E-01	-3.76E-02	-5.56E-02	-2.27E-05	-1.08E-05	-4.25E-01
$\Delta M(\text{Y})$	1.33E-04	2.10E-01	1.22E-01	-2.15E-01	-2.34E-01	2.25E-05	1.08E-05	-1.16E-01
$\Delta M(\text{CNO})$	1.10E-04	-7.94E-05	-5.29E-05	2.47E-01	2.83E-01	1.35E-06	—	5.30E-01
$\Delta M(\text{Ne+Mg})$	—	—	—	5.33E-03	6.01E-03	—	—	1.13E-02
$\delta(\text{X})$	—	—	9.27E-02	1.25E-02	7.41E-01	—	—	8.46E-01
$\delta(\text{Y})$	—	—	3.95E-02	5.40E-03	3.22E-01	—	—	3.67E-01
$\delta(\text{CNO})$	—	—	1.87E-03	2.54E-04	2.10E-02	—	—	2.31E-02
$\delta(\text{Ne+Mg})$	—	—	3.17E-04	4.30E-05	2.75E-03	—	—	3.11E-03

TABLE 1—*Continued*

	PMS	MS	RGB	He-core	AGB	Hot-WD	WD	Total
$2M_{\odot}$								
Age	7.5	1147	1203	1493	1522	1532.3	8853	
Mass	2.0	1.99	1.98	1.96	0.578	0.578	0.578	
$\log L/L_{\odot}$	1.02	1.31	1.70	1.57	2.68	0.07	-3.00	
$R$	2.84	2.24	8.16	8.27	38.8	0.0157	0.0128	
$\log T_{\text{eff}}$	3.78	3.92	3.76	3.69	3.63	4.44	3.59	
$\log g_{\text{sup}}$	3.89	4.11	3.33	2.90	2.10	7.81	7.99	—
$E_{\gamma}$	1.01E+49	2.80E+51	3.40E+50	1.31E+51	1.70E+51	1.45E+48	8.91E+47	6.16E+51
$E_{\text{NIR}}$	2.39E+48	3.87E+50	1.25E+50	4.88E+50	1.03E+51	1.59E+45	4.98E+46	2.03E+51
$E_{\text{Opt}}$	6.36E+48	1.72E+51	1.98E+50	7.81E+50	6.55E+50	2.74E+46	2.47E+47	3.36E+51
$E_{\text{UV}}$	1.36E+48	6.94E+50	1.66E+49	4.20E+49	1.42E+49	1.42E+48	5.94E+47	7.70E+50
$E_{\text{X}}$	—	—	—	—	3.52E+46	4.52E+43	—	3.52E+46
$E_{\text{H}}$	2.12E+48	2.81E+51	3.40E+50	9.82E+50	1.15E+51	2.25E+47	9.08E+46	5.28E+51
$E_{\text{He}}$	—	—	2.27E+47	3.30E+50	5.13E+50	1.44E+45	—	8.44E+50
$E_{\nu}(\text{nucl})$	1.26E+47	1.71E+50	2.29E+49	6.56E+49	7.68E+49	1.44E+46	2.45E+45	3.36E+50
$E_{\nu}(\text{ther})$	—	3.18E+43	2.50E+46	9.67E+47	8.64E+48	2.14E+48	1.61E+47	1.19E+49
$\Delta\Omega$	-1.60E+49	3.36E+48	-9.31E+47	-2.24E+48	-6.60E+49	-8.09E+48	-2.27E+48	-9.21E+49
$\Delta U$	8.00E+48	-1.64E+48	4.96E+47	1.05E+48	3.39E+49	4.73E+48	1.32E+48	4.79E+49
$\Delta M(\text{X})$	-2.14E-04	-2.34E-01	-2.95E-02	-8.45E-02	-1.06E-01	-2.03E-05	-8.44E-06	-4.55E-01
$\Delta M(\text{Y})$	6.00E-05	2.34E-01	2.93E-02	-1.37E-01	-2.40E-01	2.09E-05	8.44E-06	-1.13E-01
$\Delta M(\text{CNO})$	1.54E-04	-1.44E-04	2.03E-04	2.17E-01	3.37E-01	-1.03E-06	—	5.54E-01
$\Delta M(\text{Ne+Mg})$	—	—	—	4.80E-03	7.27E-03	—	—	1.21E-02
$\delta(\text{X})$	2.82E-05	7.46E-03	5.13E-03	1.23E-02	9.37E-01	—	—	9.62E-01
$\delta(\text{Y})$	1.10E-05	2.91E-03	2.21E-03	5.39E-03	4.14E-01	—	—	4.24E-01
$\delta(\text{CNO})$	5.53E-07	1.46E-04	1.04E-04	2.51E-04	2.66E-02	—	—	2.71E-02
$\delta(\text{Ne+Mg})$	9.41E-08	2.49E-05	1.76E-05	4.25E-05	3.50E-03	—	—	3.58E-03

TABLE 1—*Continued*

	PMS	MS	RGB	He-core	AGB	Hot-WD	WD	Total
$3M_{\odot}$								
Age	3.8	376	382	471	479.9	489.9	7816	
Mass	3.0	2.99	2.98	2.96	0.600	0.600	0.600	
$\log L/L_{\odot}$	1.76	2.02	2.26	2.07	3.11	-0.01	-3.00	
$R$	4.37	2.84	14.5	14.7	65.9	0.0150	0.0124	
$\log T_{\text{eff}}$	3.91	4.05	3.80	3.69	3.63	4.61	3.79	
$\log g_{\text{sup}}$	3.90	4.09	3.04	2.60	1.94	7.87	8.03	—
$E_{\gamma}$	2.65E+49	4.71E+51	1.23E+50	1.28E+51	1.33E+51	1.20E+48	8.78E+47	7.48E+51
$E_{\text{NIR}}$	3.70E+48	3.33E+50	3.82E+49	4.81E+50	8.26E+50	1.39E+45	4.88E+46	1.68E+51
$E_{\text{Opt}}$	1.36E+49	2.27E+51	7.15E+49	7.58E+50	5.01E+50	2.39E+46	2.46E+47	3.61E+51
$E_{\text{UV}}$	9.13E+48	2.12E+51	1.35E+49	4.01E+49	8.20E+48	1.17E+48	5.84E+47	2.19E+51
$E_{\text{X}}$	—	—	—	—	3.70E+46	4.14E+43	—	3.70E+46
$E_{\text{H}}$	1.04E+49	4.72E+51	1.29E+50	8.57E+50	8.18E+50	1.00E+47	5.28E+46	6.54E+51
$E_{\text{He}}$	—	—	1.50E+47	4.21E+50	4.86E+50	5.51E+44	—	9.07E+50
$E_{\nu}(\text{nucl})$	6.72E+47	3.23E+50	8.78E+48	5.76E+49	5.42E+49	6.40E+45	1.43E+45	4.45E+50
$E_{\nu}(\text{ther})$	—	3.84E+43	9.61E+44	6.52E+47	1.02E+49	1.91E+48	1.42E+47	1.29E+49
$\Delta\Omega$	-3.22E+49	8.12E+48	1.10E+49	-8.17E+48	-7.21E+49	-7.34E+48	-2.34E+48	-1.03E+50
$\Delta U$	1.61E+49	-3.99E+48	-5.48E+48	4.02E+48	3.69E+49	4.34E+48	1.38E+48	5.33E+49
$\Delta M(\text{X})$	-9.65E-04	-3.97E-01	-1.05E-02	-7.31E-02	-6.85E-02	-9.20E-06	-4.32E-06	-5.50E-01
$\Delta M(\text{Y})$	5.25E-04	3.97E-01	1.04E-02	-2.16E-01	-2.61E-01	9.20E-06	4.32E-06	-6.86E-02
$\Delta M(\text{CNO})$	4.58E-04	-6.34E-04	1.40E-04	2.82E-01	3.21E-01	3.54E-07	—	6.03E-01
$\Delta M(\text{Ne+Mg})$	—	—	—	6.24E-03	8.18E-03	—	—	1.44E-02
$\delta(\text{X})$	8.47E-05	1.08E-02	1.68E-03	1.50E-02	1.54E+00	—	—	1.57E+00
$\delta(\text{Y})$	3.31E-05	4.20E-03	7.11E-04	6.82E-03	7.34E-01	—	—	7.45E-01
$\delta(\text{CNO})$	1.66E-06	2.11E-04	3.38E-05	3.08E-04	7.15E-02	—	—	7.20E-02
$\delta(\text{Ne+Mg})$	2.82E-07	3.59E-05	5.73E-06	5.22E-05	7.68E-03	—	—	7.77E-03

TABLE 1—*Continued*

	PMS	MS	RGB	He-core	AGB	Hot-WD	WD	Total
$4M_{\odot}$								
Age	1.85	176	178.3	208.6	211.09	221.2	8150	
Mass	4.0	3.98	3.98	3.93	0.787	0.787	0.787	
$\log L/L_{\odot}$	2.23	2.50	2.74	2.64	3.49	0.18	-2.96	
$R$	6.37	3.30	22.2	30.6	117	0.0113	0.0102	
$\log T_{\text{eff}}$	3.97	4.13	3.87	3.68	3.61	4.64	3.84	
$\log g_{\text{sup}}$	3.85	4.08	3.03	2.11	1.47	8.23	8.32	—
$E_{\gamma}$	3.84E+49	6.71E+51	1.28E+50	1.62E+51	9.38E+50	1.84E+48	1.07E+48	9.43E+51
$E_{\text{NIR}}$	4.13E+48	2.87E+50	3.35E+49	6.49E+50	5.87E+50	8.60E+44	4.34E+46	1.56E+51
$E_{\text{Opt}}$	1.67E+49	2.47E+51	6.91E+49	9.26E+50	3.47E+50	1.51E+46	2.52E+47	3.83E+51
$E_{\text{UV}}$	1.76E+49	3.95E+51	2.53E+49	4.13E+49	4.22E+48	1.80E+48	7.69E+47	4.04E+51
$E_{\text{X}}$	—	—	—	—	3.81E+46	2.01E+46	—	5.82E+46
$E_{\text{H}}$	1.51E+49	6.72E+51	1.37E+50	1.04E+51	3.04E+50	6.34E+46	1.76E+46	8.22E+51
$E_{\text{He}}$	—	—	5.19E+47	5.74E+50	5.89E+50	3.72E+45	—	1.16E+51
$E_{\nu}(\text{nucl})$	1.04E+48	4.68E+50	9.34E+48	7.02E+49	2.04E+49	4.25E+45	4.75E+44	5.69E+50
$E_{\nu}(\text{ther})$	—	4.36E+43	5.99E+44	5.87E+47	2.66E+49	4.79E+48	1.16E+47	3.22E+49
$\Delta\Omega$	-4.65E+49	1.11E+49	1.82E+49	-1.41E+49	-1.69E+50	-1.89E+49	-3.56E+48	-2.22E+50
$\Delta U$	2.33E+49	-5.35E+48	-9.16E+48	7.18E+48	9.42E+49	1.23E+49	2.40E+48	1.25E+50
$\Delta M(\text{X})$	-1.28E-03	-5.66E-01	-1.18E-02	-8.81E-02	-2.50E-02	-5.71E-06	-2.16E-06	-6.92E-01
$\Delta M(\text{Y})$	6.72E-04	5.67E-01	1.12E-02	-3.03E-01	-3.69E-01	4.93E-06	2.02E-06	-9.31E-02
$\Delta M(\text{CNO})$	6.43E-04	-9.92E-04	4.72E-04	3.83E-01	3.91E-01	1.65E-06	—	7.74E-01
$\Delta M(\text{Ne+Mg})$	—	—	—	8.28E-03	8.75E-03	—	—	1.70E-02
$\delta(\text{X})$	1.20E-04	1.34E-02	1.85E-03	2.99E-02	2.08E+00	—	—	2.12E+00
$\delta(\text{Y})$	4.68E-05	5.24E-03	7.62E-04	1.34E-02	9.86E-01	—	—	1.01E+00
$\delta(\text{CNO})$	2.35E-06	2.63E-04	3.69E-05	6.11E-04	6.52E-02	—	—	6.61E-02
$\delta(\text{Ne+Mg})$	4.00E-07	4.48E-05	6.25E-06	1.04E-04	8.45E-03	—	—	8.60E-03

TABLE 1—*Continued*

	PMS	MS	RGB	He-core	AGB	Hot-WD	WD	Total
$5M_{\odot}$								
Age	1.04	101	102.2	117	118.055	127.0	8048	
Mass	5.00	4.98	4.97	4.89	0.838	0.838	0.838	
$\log L/L_{\odot}$	2.60	2.86	3.12	3.11	3.82	-0.43	-2.92	
$R$	7.92	3.71	33.8	52.5	196	0.0104	0.00961	
$\log T_{\text{eff}}$	4.03	4.20	3.92	3.68	3.58	4.62	3.86	
$\log g_{\text{sup}}$	3.86	4.07	3.04	1.75	1.02	8.33	8.40	—
$E_{\gamma}$	5.23E+49	8.83E+51	1.56E+50	2.29E+51	8.85E+50	1.54E+48	1.15E+48	1.22E+52
$E_{\text{NIR}}$	4.10E+48	2.57E+50	3.94E+49	9.10E+50	5.68E+50	7.08E+44	4.13E+46	1.78E+51
$E_{\text{Opt}}$	1.94E+49	2.56E+51	7.61E+49	1.31E+51	3.14E+50	1.24E+46	2.52E+47	4.28E+51
$E_{\text{UV}}$	2.88E+49	6.02E+51	4.00E+49	6.78E+49	2.99E+48	1.50E+48	8.54E+47	6.16E+51
$E_{\text{X}}$	—	—	—	—	1.54E+46	2.44E+46	—	3.98E+46
$E_{\text{H}}$	2.13E+49	8.85E+51	1.66E+50	1.51E+51	3.45E+50	6.44E+45	1.64E+45	1.09E+52
$E_{\text{He}}$	—	—	1.69E+48	7.74E+50	4.93E+50	3.44E+45	—	1.27E+51
$E_{\nu}(\text{nucl})$	1.48E+48	6.17E+50	1.14E+49	1.03E+50	2.31E+49	4.32E+44	4.43E+43	7.56E+50
$E_{\nu}(\text{ther})$	—	4.92E+43	8.72E+44	6.00E+47	4.20E+49	4.40E+48	1.21E+47	4.71E+49
$\Delta\Omega$	-6.20E+49	1.48E+49	2.45E+49	-2.16E+49	-2.03E+50	-1.84E+49	-4.11E+48	-2.70E+50
$\Delta U$	3.10E+49	-7.01E+48	-1.25E+49	1.12E+49	1.16E+50	1.25E+49	2.86E+48	1.55E+50
$\Delta M(\text{X})$	-1.89E-03	-7.41E-01	-1.25E-02	-1.28E-01	-2.80E-02	-5.36E-07	-1.23E-06	-9.11E-01
$\Delta M(\text{Y})$	1.10E-03	7.42E-01	1.13E-02	-3.82E-01	-3.07E-01	-1.14E-06	1.23E-07	6.60E-02
$\Delta M(\text{CNO})$	8.34E-04	-1.29E-03	1.22E-03	4.99E-01	3.29E-01	1.76E-06	—	8.28E-01
$\Delta M(\text{Ne+Mg})$	—	—	—	1.08E-02	7.72E-03	—	—	1.85E-02
$\delta(\text{X})$	1.27E-04	1.60E-02	2.75E-03	5.65E-02	2.53E+00	—	—	2.61E+00
$\delta(\text{Y})$	4.96E-05	6.25E-03	1.14E-03	2.50E-02	1.41E+00	—	—	1.45E+00
$\delta(\text{CNO})$	2.49E-06	3.14E-04	5.50E-05	1.15E-03	8.30E-02	—	—	8.45E-02
$\delta(\text{Ne+Mg})$	4.24E-07	5.34E-05	9.33E-06	1.95E-04	1.09E-02	—	—	1.12E-02

TABLE 1—*Continued*

	PMS	MS	RGB	He-core	AGB	Hot-WD	WD	Total
$6M_{\odot}$								
Age	0.69	65.7	66.3	74.8	75.35	83.4	7780	
Mass	6.00	5.98	5.97	5.86	0.936	0.936	0.936	
$\log L/L_{\odot}$	2.91	3.15	3.42	3.44	3.98	0.25	-2.85	
$R$	10.2	4.09	48.6	71.8	238	0.00917	0.00854	
$\log T_{\text{eff}}$	4.09	4.25	3.96	3.72	3.57	4.68	3.89	
$\log g_{\text{sup}}$	3.89	4.06	3.05	1.69	0.77	8.49	8.55	—
$E_{\gamma}$	6.86E+49	1.11E+52	1.68E+50	2.84E+51	6.57E+50	1.74E+48	1.33E+48	1.48E+52
$E_{\text{NIR}}$	4.89E+48	2.38E+50	4.27E+49	1.02E+51	4.10E+50	4.97E+44	3.64E+46	1.71E+51
$E_{\text{Opt}}$	2.20E+49	2.62E+51	7.55E+49	1.65E+51	2.45E+50	8.88E+45	2.47E+47	4.60E+51
$E_{\text{UV}}$	4.17E+49	8.25E+51	4.99E+49	1.72E+50	2.31E+48	1.64E+48	1.05E+48	8.52E+51
$E_{\text{X}}$	—	—	—	—	1.21E+46	9.25E+46	—	1.05E+47
$E_{\text{H}}$	3.00E+49	1.11E+52	1.81E+50	1.87E+51	1.92E+50	3.20E+46	9.26E+45	1.34E+52
$E_{\text{He}}$	—	—	2.57E+48	9.64E+50	4.25E+50	7.61E+44	—	1.39E+51
$E_{\nu}(\text{nucl})$	2.21E+48	7.73E+50	1.24E+49	1.27E+50	1.34E+49	2.05E+45	2.45E+44	9.28E+50
$E_{\nu}(\text{ther})$	—	5.54E+43	1.00E+45	6.37E+47	6.75E+49	6.40E+48	1.33E+47	7.47E+49
$\Delta\Omega$	-7.71E+49	1.78E+49	3.06E+49	-2.95E+49	-2.93E+50	-2.96E+49	-5.67E+48	-3.87E+50
$\Delta U$	3.85E+49	-8.32E+48	-1.57E+49	1.57E+49	1.84E+50	2.15E+49	4.22E+48	2.42E+50
$\Delta M(\text{X})$	-2.59E-03	-9.37E-01	-1.51E-02	-1.58E-01	-1.62E-02	-3.18E-06	-7.57E-07	-1.13E+00
$\Delta M(\text{Y})$	1.61E-03	9.39E-01	1.31E-02	-4.83E-01	-2.58E-01	3.18E-06	7.57E-07	2.13E-01
$\Delta M(\text{CNO})$	1.04E-03	-1.74E-03	2.00E-03	6.28E-01	2.70E-01	2.14E-08	—	8.99E-01
$\Delta M(\text{Ne+Mg})$	—	—	—	1.34E-02	5.48E-03	—	—	1.89E-02
$\delta(\text{X})$	1.83E-04	1.85E-02	3.58E-03	7.74E-02	3.00E+00	—	—	3.10E+00
$\delta(\text{Y})$	7.16E-05	7.21E-03	1.49E-03	3.40E-02	1.82E+00	—	—	1.86E+00
$\delta(\text{CNO})$	3.60E-06	3.62E-04	7.16E-05	1.57E-03	6.89E-02	—	—	7.09E-02
$\delta(\text{Ne+Mg})$	6.12E-07	6.16E-05	1.21E-05	2.66E-04	1.14E-02	—	—	1.17E-02

TABLE 1—*Continued*

	PMS	MS	RGB	He-core	AGB	Hot-WD	WD	Total
$7M_{\odot}$								
Age	0.47	46.8	47.1	52.7	53.02	60.7	6812	
Mass	7.00	6.97	6.96	6.81	1.04	1.04	1.04	
$\log L/L_{\odot}$	3.16	3.38	3.66	3.69	4.16	0.19	-2.73	
$R$	12.4	4.46	64.5	97.6	304	0.00789	0.00746	
$\log T_{\text{eff}}$	4.14	4.29	4.00	3.73	3.57	4.70	3.94	
$\log g_{\text{sup}}$	3.90	4.06	3.05	1.64	0.59	8.66	8.71	—
$E_{\gamma}$	8.39E+49	1.36E+52	1.76E+50	3.34E+51	5.80E+50	1.47E+48	1.54E+48	1.78E+52
$E_{\text{NIR}}$	5.76E+48	2.28E+50	4.44E+49	1.18E+51	3.71E+50	3.75E+44	2.98E+46	1.83E+51
$E_{\text{Opt}}$	2.44E+49	2.68E+51	7.34E+49	1.87E+51	2.08E+50	6.75E+45	2.31E+47	4.86E+51
$E_{\text{UV}}$	5.36E+49	1.07E+52	5.84E+49	2.88E+50	1.70E+48	1.31E+48	1.28E+48	1.11E+52
$E_{\text{X}}$	—	—	—	—	—	1.48E+47	—	1.48E+47
$E_{\text{H}}$	3.62E+49	1.36E+52	1.91E+50	2.41E+51	1.82E+50	1.54E+45	1.64E+45	1.62E+52
$E_{\text{He}}$	—	—	3.49E+48	1.19E+51	3.39E+50	5.93E+44	—	1.53E+51
$E_{\nu}(\text{nucl})$	2.55E+48	9.45E+50	1.31E+49	1.45E+50	1.26E+49	9.86E+44	4.43E+43	1.12E+51
$E_{\nu}(\text{ther})$	—	6.25E+43	1.10E+45	7.02E+47	1.16E+50	6.34E+48	1.44E+47	1.25E+50
$\Delta\Omega$	-9.53E+49	2.09E+49	3.65E+49	-3.80E+49	-4.47E+50	-3.37E+49	-8.14E+48	-5.67E+50
$\Delta U$	4.76E+49	-9.41E+48	-1.89E+49	2.05E+49	2.64E+50	2.59E+49	6.47E+48	3.39E+50
$\Delta M(\text{X})$	-3.31E-03	-1.15E+00	-1.62E-02	-1.78E-01	-1.60E-02	-1.20E-06	-9.50E-08	-1.36E+00
$\Delta M(\text{Y})$	2.76E-03	1.15E+00	1.35E-02	-6.2E-01	-2.08E-01	1.20E-06	9.50E-08	3.38E-01
$\Delta M(\text{CNO})$	1.24E-03	-2.16E-03	2.50E-03	7.75E-01	2.16E-01	9.00E-07	—	9.92E-01
$\Delta M(\text{Ne+Mg})$	—	—	1.18E-4	1.67E-02	5.94E-03	—	—	2.27E-02
$\delta(\text{X})$	2.47E-04	2.12E-02	4.69E-03	1.04E-01	3.43E+00	—	—	3.56E+00
$\delta(\text{Y})$	9.64E-05	8.27E-03	1.97E-03	4.55E-02	2.23E+00	—	—	2.29E+00
$\delta(\text{CNO})$	4.84E-06	4.15E-04	9.40E-05	2.11E-03	8.02E-02	—	—	8.29E-02
$\delta(\text{Ne+Mg})$	8.24E-07	7.06E-05	1.59E-05	3.58E-04	1.34E-02	—	—	1.39E-02



TABLE 1—*Continued*

	PMS	MS	RGB	He-core	AGB	Hot-WD	WD	Total
$8M_{\odot}$								
Age	0.33	35.4	35.6	39.6	39.94	47.73	4811	
Mass	8.0	7.97	7.94	7.54	1.15	1.15	1.15	
$\log L/L_{\odot}$	3.37	3.58	3.86	3.88	4.17	0.14	-2.56	
$R$	14.8	4.82	79.3	136	300	0.00645	0.00619	
$\log T_{\text{eff}}$	4.17	4.32	4.04	3.71	3.57	4.74	4.02	
$\log g_{\text{sup}}$	3.88	4.05	3.08	1.43	0.50	8.88	8.92	—
$E_{\gamma}$	9.54E+49	1.63E+52	1.82E+50	3.65E+51	5.95E+50	1.25E+48	1.57E+48	2.09E+52
$E_{\text{NIR}}$	6.46E+48	2.23E+50	4.42E+49	1.43E+51	3.59E+50	2.55E+44	1.90E+46	2.06E+51
$E_{\text{Opt}}$	2.55E+49	2.76E+51	7.03E+49	1.96E+51	2.34E+50	4.66E+45	1.73E+47	5.05E+51
$E_{\text{UV}}$	6.34E+49	1.34E+52	6.71E+49	2.62E+50	2.14E+48	9.89E+47	1.38E+48	1.37E+52
$E_{\text{X}}$	—	—	—	—	—	2.56E+47	—	2.46E+47
$E_{\text{H}}$	3.89E+49	1.64E+52	1.97E+50	2.18E+51	5.60E+49	7.32E+45	1.43E+43	1.88E+52
$E_{\text{He}}$	—	—	4.34E+48	1.43E+51	4.96E+50	—	—	1.93E+51
$E_{\text{C}}$	—	—	—	—	2.87E+50	—	—	2.87E+50
$E_{\nu}(\text{nucl})$	2.72E+48	1.13E+51	1.36E+49	1.49E+50	6.78E+48	4.68E+44	3.86E+41	1.30E+51
$E_{\nu}(\text{ther})$	7.04E+43	1.16E+45	8.08E+47	6.78E+48	4.58E+50	6.94E+48	1.61E+47	4.66E+50
$\Delta\Omega$	-1.13E+50	2.40E+49	4.15E+49	-4.73E+49	-7.49E+50	-4.83E+49	-1.17E+49	-9.05E+50
$\Delta U$	5.65E+49	-1.07E+49	-2.16E+49	2.56E+49	5.33E+50	4.01E+49	9.92E+49	5.65E+50
$\Delta M(\text{X})$	-3.59E-03	-1.39E+00	-1.66E-02	-1.85E-01	-4.39E-02	-5.64E-07	-9.40E-08	-1.64E+00
$\Delta M(\text{Y})$	2.23E-03	1.39E+00	1.36E-02	-6.42E-01	-2.54E-01	5.64E-07	9.40E-08	5.09E-01
$\Delta M(\text{CNO})$	1.44E-03	-2.14E-03	2.75E-03	8.09E-01	-6.83E-02	—	—	7.43E-01
$\Delta M(\text{Ne+Mg})$	—	—	2.40E-04	1.77E-02	3.09E-01	—	—	3.27E-01
$\delta(\text{X})$	2.75E-04	2.41E-02	1.52E-02	1.21E-01	3.61E+00	—	—	3.93E+00
$\delta(\text{Y})$	1.07E-04	9.40E-03	6.46E-03	5.63E-03	2.66E+00	—	—	2.79E+00
$\delta(\text{CNO})$	5.40E-06	4.72E-04	3.05E-04	9.55E-04	8.82E-02	—	—	9.46E-02
$\delta(\text{Ne+Mg})$	9.18E-07	8.03E-05	5.17E-05	9.55E-04	1.49E-02	—	—	1.60E-02

TABLE 2  
EVOLUTIONARY CHARACTERISTICS OF A  $0.8M_{\odot}$  STAR.

	PMS	MS	RGB
$0.8M_{\odot}$			
Age	73.2	25560	30211
Mass	0.8	0.798	0.709
$\log L/L_{\odot}$	-0.45	-0.40	0.77
$R$	0.90	0.81	2.27
$\log T_{\text{eff}}$	3.66	3.70	3.70
$\log g_{\text{sup}}$	4.51	4.54	4.10
$E_{\gamma}$	3.01E+48	1.22E+51	3.07E+51
$E_{\text{NIR}}$	1.32E+48	4.33E+50	1.85E+51
$E_{\text{Opt}}$	1.63E+48	7.42E+50	1.44E+51
$E_{\text{UV}}$	5.64E+46	4.65E+49	3.98E+49
$E_{\text{X}}$	—	—	—
$E_{\text{H}}$	9.31E+47	1.22E+51	3.05E+51
$E_{\text{He}}$	—	—	1.73E+47
$\Delta\Omega$	-4.16E+48	-2.40E+47	-3.83E+49
$\Delta U$	2.08E+48	1.33E+47	2.46E+49
$E_{\nu}(\text{nucl})$	2.38E+46	2.99E+49	2.01E+50
$E_{\nu}(\text{ther})$	—	1.66E+43	2.82E+47
$\Delta M(\text{X})$	-1.31E-04	-9.71E-02	-2.40E-01
$\Delta M(\text{Y})$	1.32E-04	9.70E-02	2.40E-01
$\Delta M(\text{CNO})$	8.86E-07	1.40E-04	-2.55E-04
$\Delta M(\text{Ne+Mg})$	—	—	—
$\delta(\text{X})$	—	1.16E-03	6.22E-02
$\delta(\text{Y})$	—	4.52E-04	2.57E-02
$\delta(\text{CNO})$	—	2.27E-05	1.24E-03
$\delta(\text{Ne+Mg})$	—	3.86E-06	2.11E-04

TABLE 3  
MEAN VALUES OF  $R$  AND  $K$ .

$M$	$R(\text{MS})$	$K(\text{MS})$	$R(\text{RGB})$	$K(\text{RGB})$	$R(\text{He-core})$	$K(\text{He-core})$	$R(\text{WD})$	$K(\text{WD})$
0.8	0.806	1.382	2.265	2.610	-	-	-	-
1	1.000	1.594	2.603	2.601	9.743	59.81	0.0138	0.927
1.5	1.790	2.300	10.02	5.587	10.75	27.57	0.0130	0.927
1.8	2.108	2.328	15.62	7.385	10.13	13.39	0.0131	0.925
2	2.239	2.291	8.158	4.072	8.276	6.981	0.0128	0.925
3	2.844	2.148	14.55	4.795	14.71	7.758	0.0125	0.925
4	3.302	2.036	22.16	4.974	30.62	13.36	0.0102	0.942
5	3.709	1.954	33.83	5.006	52.49	20.76	0.0096	0.949
6	4.095	1.900	48.58	5.097	71.80	23.57	0.0085	0.967
7	4.463	1.858	64.50	5.151	97.65	26.59	0.0074	0.993
8	4.821	1.825	79.34	5.123	135.82	35.69	0.0061	1.033